JOURNAL OF PETROLOGY | VOLUME 44 | NUMBER 7 | PAGES 1193–1210 | 2003

Melt Dynamics of a Partially Molten Mantle with Randomly Oriented Veins

S. MAALØE*

GEOLOGISK INSTITTUTT, UNIVERSITAS BERGENSIS, ALLEGATEN 41, 5007 BERGEN, NORWAY

RECEIVED MAY 6, 2002; ACCEPTED FEBRUARY 11, 2003

The statistical probability of a connected network of randomly oriented melt veins in partially molten mantle suggests that the critical melting model can account for observed ($^{226}Ra/^{230}Th$) isotope activity ratios. Similarly, if the reactive percolation model also includes such veins, then this modified model is also relevant. Critical melting models for the isotope activity ratios imply that material exchange between the melt and the residuum must be negligible. Hence, any diffusive exchange between the melt in the veins and the residuum must be limited. This condition suggests that the veins form a rooted system where several smaller veins supply larger veins. Further, the veins should be situated at least some decimetres apart, and the permeability constant of the residuum should be larger than $\sim 10^{-10}$ cm^2. These conditions ensure that diffusion does not change the composition of the residuum significantly. Using isotope activity ratios alone, it is difficult to distinguish between the percolative and critical melting models, because both can account for the observed data. The concentrations of incompatible elements in residual harzburgites and other evidence appear to favour the critical melting model. It is suggested that veins can form as the result of overpressure caused by an interstitial melt, because of the volume expansion during melting.

KEY WORDS: *basalts; isotopes; magma accumulation*

INTRODUCTION

The earliest stages of accumulation of basaltic melt within partially molten mantle must occur by a process of percolation, in which the melt migrates along interstices between the grains and reacts with the residuum. With increasing degree of melting the melt either may continue to migrate by percolation or may start to form veins. If veins are formed, the majority of the melt accumulation occurs by flow in the veins, as flow in veins is faster than interstitial percolation. Some melting models assume that the melt migrates entirely by interstitial percolation, either through a permeable matrix or through channels with a large permeability (McKenzie, 1985; Ceuleneer & Rabinowicz, 1992; Spiegelman & Elliot, 1993; Lundstrom *et al*., 1995; Kelemen *et al*., 1997). Other models assume that the percolating melt accumulates in veins, and that the main part of the melt extraction occurs by flow in veins (Wood, 1979; Maaløe, 1982; Sleep, 1988; Cortini, 1990; Hart, 1993; Richardson & McKenzie, 1994).

The isotope activity ratio ($^{226}Ra/^{230}Th$) of basalts can be used to constrain models for partial melting of the mantle; however, the observed ratios can be explained in different ways. There are two basic models. The percolation model is a reaction model that assumes that the melt ascends interstitially whilst reacting with the residuum. The critical model is a non-reaction model that assumes that the melt is extracted from the residuum and ascends in veins without significant reaction with the residuum (Maaløe, 1982; McKenzie, 1985; Maaløe & Johnston, 1986). Theoretical considerations by Iwamori (1994) and Sims *et al*. (1999) of isotope activity ratios in Hawaiian basalts allow for both percolation and flow in veins. The geochemistry of mid-ocean ridge basalt (MORB) suggests that most melt extraction is in chemically isolated conduits according to Kelemen *et al*. (1997). A more complex model, involving the mixing of melts derived from reactive low-porosity and non-reactive high-porosity sources, was, however, suggested by Sims *et al*. (2003) for the East Pacific Rise. An entirely different model assumes that the ascent of melt takes place in cylindrical channels surrounded by a porous matrix, as proposed by Richardson *et al*. (1996), who concluded

*E-mail: Sven.Maaloe@geo.uib.no

that the melt propagates slowly upwards as solitary waves.

It was suggested by Richardson & McKenzie (1994) that equilibrium percolation cannot explain the observed ($^{226}Ra/^{230}Th$) activity ratios for MORB of ~2·00, because percolation through the spinel lherzolite field would result in too slow ascent rates. The melts generated within the garnet lherzolite field must, therefore, ascend in dykes through the spinel lherzolite stability field without reacting with the surrounding spinel lherzolite. The intrusion of batches of magma into the abyssal magma chambers indicates that the melts must have been accumulated within their sources. The melts generated within the garnet lherzolite field must have been accumulated before they ascended. Percolation does not result in magma accumulation, because the melt remains within the interstices. This suggests that the melts must accumulate via a network of veins before they can ascend. The observed ranges of isotope activity ratios for MORB were modelled by Spiegelman & Elliot (1993) assuming interstitial percolation. Their modelling implies a permeability constant k as large as 10^{-4} cm^2, whereas experimental analogues and theoretical modelling suggest that k is $<10^{-9}$ cm^2 (Maaløe & Scheie, 1982; von Bargen & Waff, 1986; Richardson & McKenzie, 1994). This discrepancy could suggest that percolation is not a relevant melting mode; however, if veins are formed in the residuum, then the permeability of the residuum will be increased significantly as shown in a subsequent section. Hence, if it is assumed that the melt in such veins reacts with the residuum, then such a veined percolation model becomes relevant.

Evidence for critical melting has been obtained from the compositions of clinopyroxene in residual lherzolites (Johnson *et al.*, 1990; Hellebrand *et al.*, 2001), and from rare earth element concentrations in peridotites from ophiolite complexes (Batanova *et al.*, 1998; Batanova & Sobolev, 2000). The compositions of melt inclusions in olivine phenocrysts in tholeiites from the Mid-Atlantic Ridge are also consistent with a critical mode of melting (Sobolev & Shimizu, 1993). The presence of 2% interstitial melt in abyssal peridotite generated by fractional melting was inferred from textural evidence by Seyler *et al.* (2001). Apparently, therefore, some evidence favours a critical melting mode.

Although different melt accumulation models have been proposed, all of these models suggest that the percentage of interstitial melt in the residuum must be small, less than ~1% (Salters & Longhi, 1999). Further, the models imply that the mantle must become permeable when less than ~1% melt has been generated. Accepting such small percentages of interstitial melt and the critical melting model, it follows that a connected network of veins must begin to form soon after the mantle becomes permeable. This study considers the statistical probability and dynamics of such a connected network of veins.

There is little direct or indirect evidence available that reveals the structure of the partially molten mantle, and any model, including the vein model presented here, must be considered hypothetical. The vein model is considered here because a veined mantle results in a much faster ascent rate of the melt than by percolation. The vein model also allows for a spatial separation between the melt and the residuum. The most deep-seated evidence for magma transfer is obtained from eclogite and websterite veins in peridotite nodules (Wilshire & Kirby, 1989). In addition, websterite veins and dykes are present in lherzolite massifs, as well as in mantle peridotites from ophiolite complexes (Kornprobst, 1969; Dikey, 1970; Conquéré, 1977; Schubert, 1977; Boudier, 1978; Quick, 1981; Bodinier *et al.*, 1987; Amundsen *et al.*, 1988; Python & Ceuleneer, 2003). Even if the presence of eclogite and websterite veins in peridotites does not indicate the structure of the partially molten mantle, their presence shows that veins can at least form in a deep-seated and hot part of the mantle.

Theoretical considerations suggest that hydraulic fractures can form by liquid overpressure in a permeable medium (Geertsma & de Klerk, 1969), so that vein formation in partially molten peridotite may be possible, as suggested by Rubin (1998). The orientation of the veins may be random, or if shear controls the vein formation they may be parallel. The orientation depends on the flow pattern within the mantle. Sheared flow will induce parallel veins as seen in the La Ronda massif (Dikey, 1970; Stevenson, 1989). However, these veins are not generally connected by apophyses (G. Ceuleneer, personal communication, 2002), so that sheared flow does not necessary result in a connected network of veins. Other lherzolite massifs, such as the Horoman, Fontête Rouge and Lherz massifs, have sub-parallel layers of harzburgite and lherzolite, which suggest melt accumulation either by compaction or shear (Conquéré, 1977; Bodinier *et al.*, 1987; Obata & Nagahara, 1987; Bodinier *et al.*, 1990; Takazawa *et al.*, 2000). The melt channels in peridotites from ophiolite complexes have arbitrary orientations and the distances between them are of the order of decimetres (Ceuleneer & Rabinowicz, 1992). These melt channels are considered porous channels rather than veins (G. Ceuleneer, personal communication, 2000). The orientation of the veins assumed present in a partially molten mantle must at present be considered unknown. A basic model assuming arbitrarily oriented veins is therefore considered as a starting point, which shows some of the essential features of a veined mantle source.

Some definitions of the terms and parameters used here is considered relevant. The term 'vein' is used for a crack filled with melt. A 'residuum' may consist of a permeable part with interstitial melt only and veins. The permeable part is here called the 'matrix' to distinguish it from the entire residuum. 'Permeability' is generally used to describe the flow resistance in porous media; however, it is convenient to estimate the permeability of a veined source, because the equations applied for permeable flow then also can be applied for a source with randomly oriented veins (Long *et al.*, 1982).

The pressure of the melt exceeding lithostatic pressure is here called the overpressure. If the lithostatic pressure is P_l and that of the melt is P_m, then the overpressure of the melt is $\Delta P = P_m - P_l$. The formation of veins is possible only if the melt has an overpressure, i.e. if $\Delta P > 0$. Taking the density of the mantle as 3·3 g/cm^3 and that of the melt as 3·0 g/cm^3 at high pressures, then the pressure gradient of the melt becomes 30 bar/km (Boyd & McCallister, 1976; Scarfe *et al.*, 1979). The viscosity of the melt is taken to be 10 poise (1 Pa s) based on the experimental results for olivine tholeiite of Scarfe *et al.* (1979).

The melt generation rate is estimated using the phase relations for peridotite of Walter (1998) and the heats of fusion of Richet & Bottinga (1986), except for forsterite, for which the heat of fusion of Robie & Waldbaum (1968) was used. At 30 kbar a melt generated by 24 wt % melting contains 18·22% MgO at 1540°C. Assuming a specific heat of 0·25 cal/°C g the formation of such a melt would be associated with a temperature drop of 140°C, neglecting the adiabatic temperature drop. Thus the initial temperature must have been 1680°C, which is the solidus temperature at 56 kbar. Neglecting the possible effect of fluids, melting in the mantle is initiated at a depth of ~170 km, partly in accordance with the theoretical convection model of Ceuleneer *et al.* (1993), which estimated this depth as ~150 km. Their model assumes the temperature of the core of the convection cell is 1280°C, equal to the mean mantle potential temperature estimated by McKenzie & Bickle (1988). Melt generation corresponds to a pressure decrease of 26 kbar and an ascent distance of 79 km. The weight fraction of the melt therefore increases by $3{\cdot}04 \times 10^{-8}$ cm^{-1}. For an ascent rate of 10 cm/a the annual melt generation rate is then estimated as $3{\cdot}04 \times 10^{-7}$ a^{-1}.

The equation relating the permeability, k cm^2, to the volume fraction of interstices f has been estimated by an experimental analogue as (Maaløe & Scheie, 1982)

$$k = \frac{f^2 d^2}{6400} \tag{1}$$

where d is the grain diameter in centimetres. The permeabilities estimated from this equation are ~10 times larger at 1% melt than those derived from a theoretical estimate by von Bargen & Waff (1986), the exact difference depending on the assumed wetting angle. The percolative flux $\mathcal{J}$ cm^3/cm^2 s is estimated by Darcy's law:

$$\mathcal{J} = -\frac{k}{\eta}\frac{\mathrm{d}P}{\mathrm{d}z} \tag{2}$$

where η is viscosity, and $\mathrm{d}P/\mathrm{d}z$ is the pressure gradient for the interstitial melt, here taken as 30 bar/km.

PROBABILITIES OF VEIN INTERSECTION

Intersection between two veins

The statistical relationships of randomly oriented veins are estimated as follows. If the intersection probability between two veins is ρ then the intersection probability, R, between n veins is

$$R = \rho^{n-1}. \tag{3}$$

The probability ρ varies between 0 and 1·00. For a probability of $\rho = 0{\cdot}5$, the intersection probability between 10 veins becomes as small as $9{\cdot}8 \times 10^{-4}$. If 1000 veins are present one array of 10 veins may be connected. This example show that the vein density must be large before the partially molten lherzolite attains a large permeability. This relationship is demonstrated in Fig. 1 for a two-dimensional (2D) case where lines of arbitrary positions, orientations and lengths intersect. For a small line density the number of intersections between several lines is zero, and a large density is required before several lines are connected as shown by Hestir & Long (1990).

The intersection probability for the 2D case with intersecting lines is estimated by geometrical construction and is shown in Fig. 2. The probability curve is approximated by the three-parameter sigmoidal curve given by

$$\rho = \frac{a}{1 + \mathrm{e}^{-(x-c)/b}} \tag{4}$$

where $a = 0{\cdot}9627$, $b = -0{\cdot}2220$ and $c = 0{\cdot}8479$. The intersection probability for the 3D case is here estimated for two circular planes with the same and different radii (Fig. 3). One circular plane is a reference plane and is kept in a constant position and orientation, whereas the other plane is tilted and its distance is varied relative to the reference plane. The distance between the circular planes is defined as the distance between the centres of the circular planes. The intersection probability is estimated by letting the tilting plane tilt 10° about its x-axis; thereafter the plane rotates 90° in 10° steps around its y-axis. The

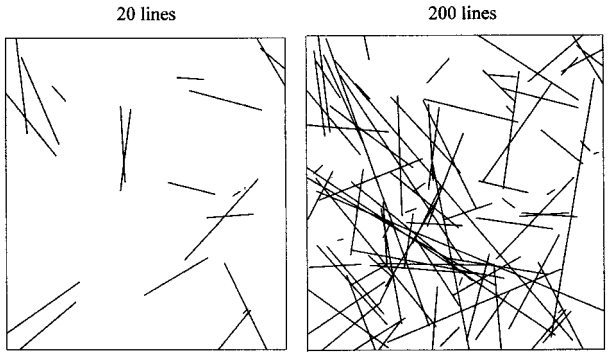

Fig. 1. The distribution of 20 and 200 lines with arbitrary lengths, orientations and positions. The method used for arbitrary number generation is the multiplicative linear congruential method. Intersections between several such arbitrary lines are possible only if the density of the lines is relatively large compared with their length.

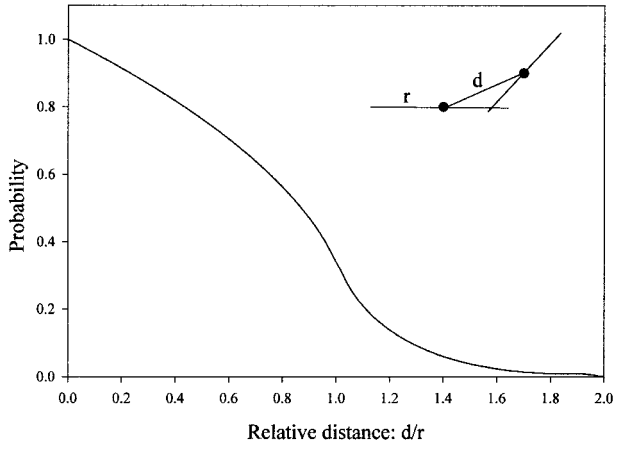

Fig. 2. The probability of intersection between two lines as function of their relative distance, $x = d/r$. The lengths of the two lines are the same. The probability of intersection is large for small distances, and small when the distance is more than one length unit.

tilting plane is then rotated 360° around the z-axis and the angle of intersection with the stationary plane circle estimated. If the angle of intersection is φ then the probability of intersection is φ/360. The intersection probability varies not only with distance between the planes but also with their relative positions. For each chosen distance d the position is varied in 10° steps so that $x = d\cos(\gamma)$, and $y = d\sin(\gamma)$, where γ is the position angle varying from 0° to 90°. For each distance chosen the probability is therefore estimated for 10 relative positions, and 100 different orientations of the tilting plane, so that the probability for each distance is estimated from 1000 intersections. The variation in intersection probability with distance for two circular planes with the same radius is shown in Fig. 4. The probability curve is somewhat similar to the 2D curve, shown in Fig. 3. The 3D probability

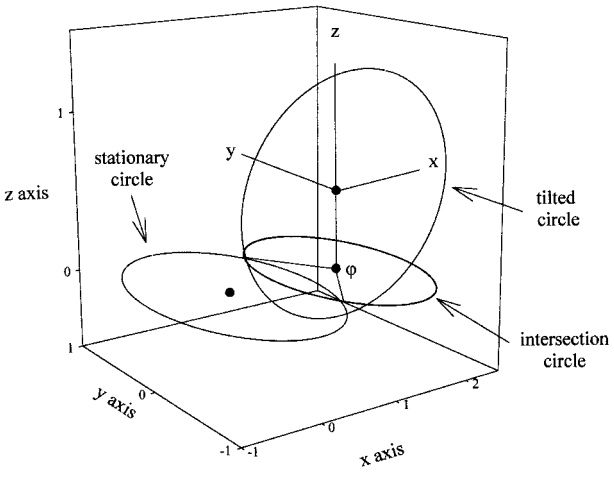

Fig. 3. An illustration of how the intersection probability is estimated for two circular planes with the same diameter. The tilting circle is here tilted 45° around its y-axis and its centre has the coordinates $x = 1{\cdot}5$ and $y = 0{\cdot}5$. The angle of intersection is obtained by rotation around the z-axis and is shown by φ.

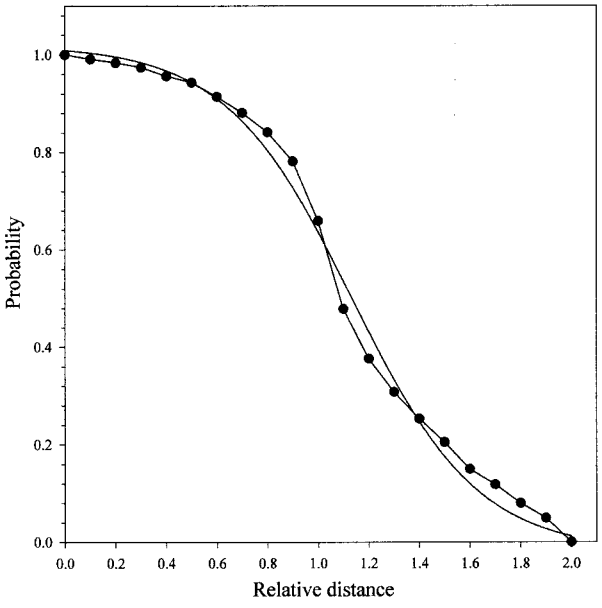

Fig. 4. The intersection probability as a function of the relative distance for two circular planes with the same radii. The dots show the calculated intersection probabilities. The smooth curve is the approximation obtained using a four-parameter sigmoidal curve equation (5).

curve is approximated by the addition of a four-parameter sigmoidal curve to a linear one, and is given by

$$\rho = c + \frac{a}{1 + e^{-(x-d)/b}} + \alpha x + \beta \qquad (5)$$

where x is the relative distance between the centres of the circular planes. If the distance between the centres

Table 1: Constants for the probability equation (5) for varying radii of the tilting circle

Radius	*a*	*b*	*c*	*d*	α	β
0·1	11·4675	−0·1955	0·0006	−0·4563	0·0083	−0·0137
0·2	5·8132	−0·3435	0·0003	−0·5162	0·0159	−0·0584
0·3	1·8351	−0·3331	−0·0089	0·1171	0·0200	−0·0861
0·4	1·3671	−0·3206	−0·0176	0·4179	0·0101	−0·0575
0·5	1·2093	−0·3026	−0·0196	0·6068	0·0039	−0·0462
0·6	1·1294	−0·2825	−0·2000	0·7557	0·0015	−0·0366
0·7	1·0695	−0·2590	−0·0146	0·8833	−0·0049	−0·0207
0·8	1·0338	−0·2418	−0·0043	0·9790	−0·0097	−0·0118
0·9	1·0038	−0·2329	0·0123	1·0506	−0·0172	−0·0052
1·0	0·9614	−0·2076	0·0368	1·1091	−0·0281	0·0064

of the planes is l, and r_1 the radius of the stationary circle, then $x = l/r_1$. The first two terms are obtained by the approximation to a sigmoidal curve. This curve deviates slightly from $\rho = 1$ at $x = 0$, and at $\rho = 0$ for $l = r_1 + r_2$, where r_2 is the radius of the tilting circle (Fig. 4). The two last linear terms correct for this deviation. When the two circles have the same radius the constants are given by: $a = 0{\cdot}9614$; $b = -0{\cdot}2076$; $c = 0{\cdot}0368$; $d = 1{\cdot}1092$; $\alpha = -0{\cdot}0281$; $\beta = 0{\cdot}0064$. The constants for varying radii of the tilting circle are shown in Table 1, and the probability curves are shown in Fig. 5. This probability equation represents an approximation to the intersection probability of real veins, because it assumes a planar circular shape of the veins. The veins in partially molten lherzolite are probably somewhat irregular in shape, which increases their intersection probability compared with that of planar surfaces.

Number of arrays of connected veins

The vein density, i.e. the number of veins per cubic unit, depends on the assumed amount of melt present in the veins, the distance between the veins, and the thickness of the veins; the thinner the veins the larger their number. The shape of the veins is here considered as a rotation ellipsoid with radius r cm and half-height h cm. The veins are considered thin with $h = 0{\cdot}001r$ or $h = 0{\cdot}01r$. The volume of a vein is then given by

$$v = \frac{4}{3}\pi h r^2. \tag{6}$$

If the volume fraction of melt in the veins is g, and the unit volume $1\,\mathrm{m}^3$, the unit volume then contains $m = g \times 10^6\,\mathrm{cm}^3$ melt in the veins. The number of veins is then given by

$$N = m/\nu. \tag{7}$$

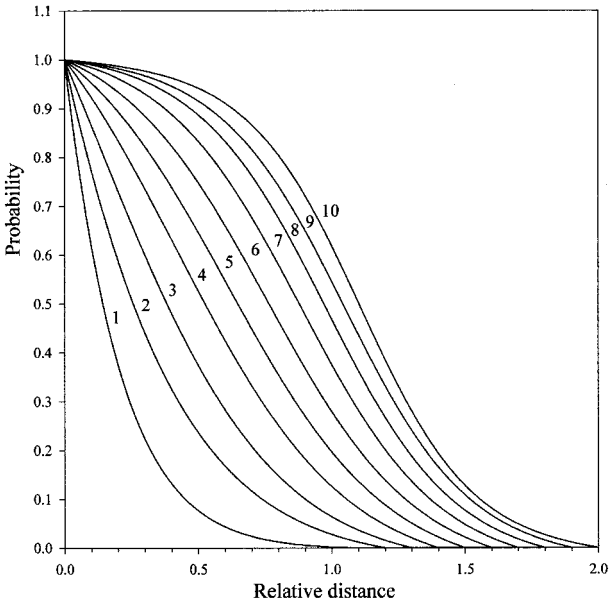

Fig. 5. The variation in intersection probability as a function of relative distance for two circular planes with different radii. The stationary plane has a constant radius $r = 1{\cdot}00$, and the tilting plane has radius varying from $0{\cdot}1r$ to $1{\cdot}0r$, identified by the numbers 1–10. The curves are estimated using equation (5) and the constants in Table 1.

The average distance between the centres of the veins is then estimated from

$$l = \left(\frac{10^6}{N}\right)^{1/3} \tag{8}$$

thereafter the intersection probability between a pair of veins is estimated from (5) for $x = l/r$. Considering that the orientation of veins is taken as being random, the number of veins needed for intersection over a distance of 100 cm is estimated assuming an average orientation of 45° along an array of average intersections at $\frac{1}{2}r$. The number of veins needed for connection across the $1\,\mathrm{m}^3$ reference volume is therefore approximately given by $M = 100/r\sin(45°)$. Using (3), the probability of a 1 m long array of connected veins is then given by

$$R = \rho^{M-1} \tag{9}$$

and the number of such arrays in $1\,\mathrm{m}^3$ is given by

$$W = RN. \tag{10}$$

The number of connected arrays of veins decreases with increasing size as shown in Fig. 6, but the number is fairly similar for the different sizes for $<1\%$ melt in the veins. At $\sim 0{\cdot}5\%$ melt in the veins, the number of connected arrays varies from about 1 to 100 with decreasing vein size. This range appears sufficient for efficient melt extraction.

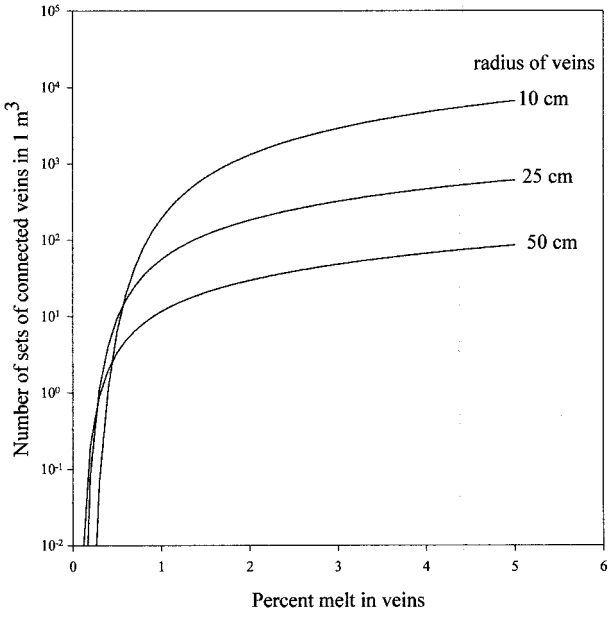

Fig. 6. The number of sets of connected veins in 1 m^3 for veins with constant radii of 10 cm, 25 cm, and 50 cm, as a function of the percentage of melt present in the veins.

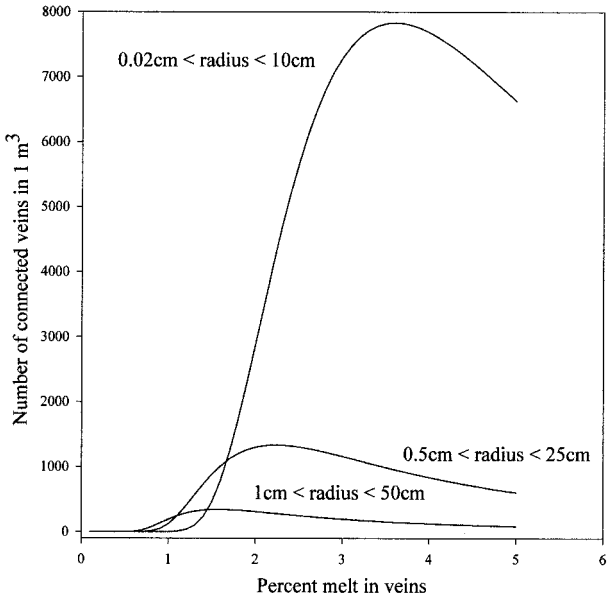

Fig. 7. The number of sets of veins that are connected over a 1 m distance in 1 m^3 residuum as a function of the percentage of melt present in the veins. The same diagram applies for other length- and volume-scales. The diagram applies for a linear increase in vein radius with increasing amount of melt. The number of connected veins is shown for three size ranges of the veins. Connectivity begins slightly below 1% melt, suggesting that melt can be extracted from a partially molten source with ~1% melt or slightly less. In this diagram the half thickness of the veins, h, equals $0{\cdot}001r$. The same diagram is shown in Fig. 8 for $h = 0{\cdot}01$.

It is possible that the size of the veins increases with the amount of melt present. The variation in W is shown in Fig. 7 for a linear increase in the vein size with the total amount of melt present in the veins. The number of intersecting veins attains a pronounced maximum for small veins, whereas larger veins result in a less pronounced maximum. The maxima arise because the probability of intersection increases with their number, which on the other hand decreases with their size. According to Fig. 7, the number of arrays of connected veins over a distance of 100 cm in the presence of 1% melt in the veins is 0·98, 122, and 191/m^3 for maximal radii of 10, 25, and 50 cm, respectively. If this estimate is representative it means that their maximal radius is probably >10 cm. The significant feature of Figs 5 and 6 is that vein connectivity appears possible even in the presence of only 1% melt in the veins. This percentage must be larger than the degree of melting, because some melt also must be present in the interstices; however, the accumulation of melt at degrees of melting of ~1% appears possible. In these estimates the half-width of the veins is $0{\cdot}001r$, where r is the radius of the veins. For $h = 0{\cdot}01r$ the number of connected veins is much smaller and connectivity with just one connected set of veins does not arise before the melt percentage is larger than 3% (Fig. 7). For efficient connectivity the number of connected veins must be $>1/m^3$. This result therefore suggests that during the initial stages of partial melting the veins must be thin.

The average distance between the centres of the veins varies with the amount of melt present. For veins with radii of 25 and 50 cm, the centre-to-centre distances are about 3 and 7 cm, respectively, in the presence of 1% melt in the veins, and $h = 0{\cdot}001$ (Fig. 8). The interstitial melt must thus have to migrate only for a rather short distance before it ends up in a vein.

DIFFUSIVE EXCHANGE

The critical melting model assumes that the melt does not exchange components with the residuum during ascent. If the concentration of incompatible elements is increased in the residuum by diffusion from the veins, then the melting approaches percolative melting, because the enriched part of the residuum undergoes further melting during subsequent ascent. A diffusive exchange between the melt in the veins and the residuum is prevented if the flow rate of melt from the matrix into the veins is large compared with the opposite diffusion rate from the melt in the vein into the interstitial melt in the matrix.

At a given height in the mantle above the onset of partial melting the melt in the veins attains a constant concentration because melt is flowing up through the

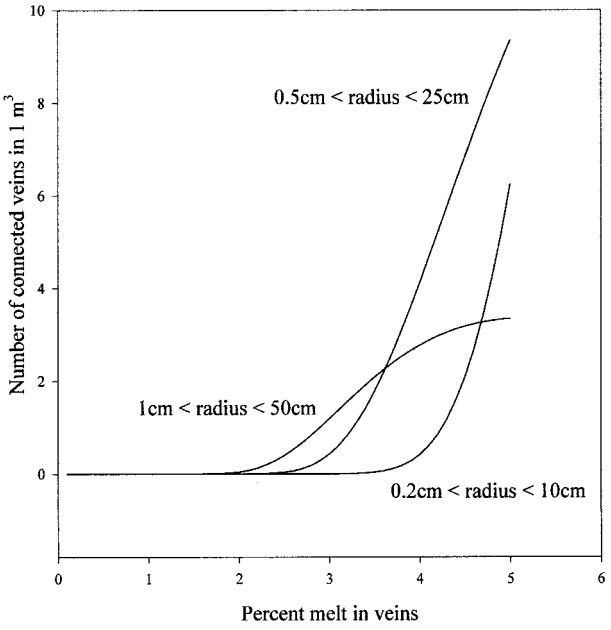

Fig. 8. The number of sets of connected veins as in Fig. 7, but with $h = 0{\cdot}01$. The number of sets is much smaller, suggesting that the veins that initially form must be very thin.

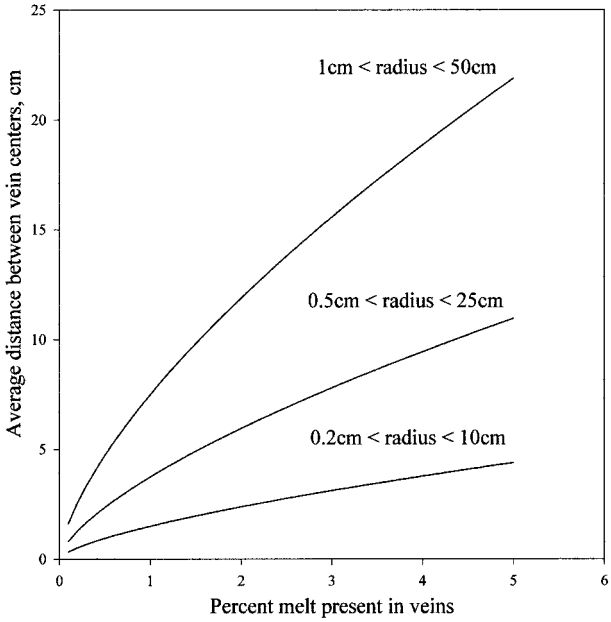

Fig. 9. The average distances between veins as a function of percentage melt and their size ranges for $h = 0{\cdot}001$. The distances are small. Larger distances are obtained if the veins have larger sizes and smaller veins are absent.

veins. The diffusion distance is therefore estimated by using the diffusion equation for a semi-infinite sheet, where the concentration is constant at $x = 0$, and x is the distance from the vein. The melt in interstices flows in the opposite direction to diffusion, and the steady-state equation for a moving boundary is therefore used (Chalmers, 1964):

$$C(x) = C_0 \exp\left(\frac{-Rx}{D}\right) \qquad (11)$$

where $C(x)$ is concentration at distance x from the vein, C_0 is the concentration in the vein, D is diffusion coefficient, and R is the constant flow rate of melt within the interstices (cm/s). An appropriate D value at 1550°C is $D = 10^{-5}$ cm^2/s (Hofmann, 1980). By critical melting the concentration of a trace element with $D = 0{\cdot}001$ in a residuum situated near a vein is 10–20 ppm larger than the concentration of the residuum before diffusion took place (Maaløe & Johnston, 1986). The effect of diffusion is here illustrated by normalizing this difference by letting $C_0 = 1$. As shown in Fig. 10, the concentration profiles depend on the assumed value of the permeability constant, k, because the flow rate of the melt, R, depends on k. The diffusion mainly takes place within the interstices, because the diffusion rate within the mineral grains is very small. The change in the bulk composition of the residuum will therefore be $1/f$ times smaller than (11) and Fig. 10 suggest. For $f = 0{\cdot}01$, the change in bulk composition is therefore 100 times smaller.

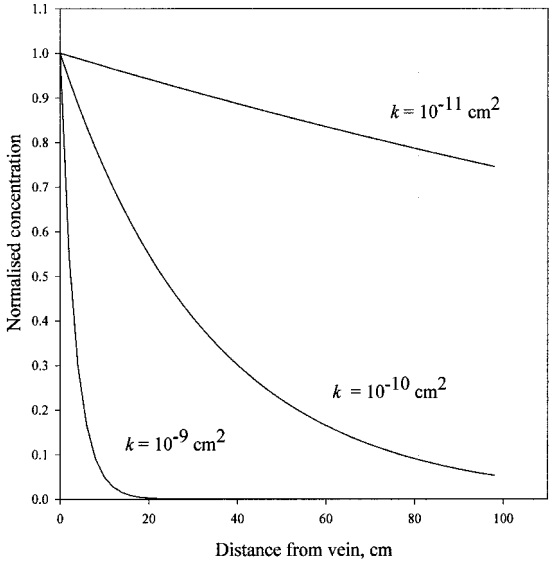

Fig. 10. Steady-state diffusion profiles in the residuum for different permeabilities, k. The variation in concentration is estimated assuming 1% interstitial melt, i.e. $f = 0{\cdot}01$, and a diffusion coefficient equal to 10^{-5} cm^2/s. The change in the bulk composition of the residuum will be 100 times smaller, because $f = 0{\cdot}01$.

The concentration profiles in Fig. 10 show that diffusion from a vein does take place, and that the change in the composition of the residuum depends on the permeability of the residuum. For a fraction of melt in the

interstices given by $f = 0{\cdot}01$, and a grain size 0·1 cm, $k = 1{\cdot}5 \times 10^{-10}$ cm^2 using (1), and the flux of melt from the interstices is 0·14 cm/a. The melt migration rate within the interstices is $1/f$ larger, i.e. 14 cm/a, but still relatively small compared with the steady-state diffusion distances. Although (1) may result in approximate estimates of the permeability constant, it must be emphasized that the permeability of partially molten peridotite is not known with sufficient accuracy for an estimate of the diffusion distance. For a permeability constant equal to or larger than 10^{-10} cm^2 the steady-state diffusion distance is less than a few decimetres, and the change in the bulk composition of the residuum will be insignificant if the distances between the veins are more than this distance.

The change in the composition of the residuum by diffusion may be insignificant if the veins start to form a rooted system, where small veins supply larger veins that supply still larger veins or dykes that are situated several metres apart. The composition of the residuum along the largest veins or dykes will change by diffusion, but the change in the average composition of the entire residuum will be small if these veins are situated metres apart. Consequently, for a vein model to be consistent with the critical melting model, the veins should probably form a network where smaller veins supply still larger ones, so that a rooted network is formed.

INTERSECTION PROBABILITY FOR A ROOTED NETWORK

A rooted network has previously been suggested by Hart (1993), who considered a fractal network with tubular channels. The network envisaged here is instead a network of interconnected circular disks with elliptical cross-sections. In a rooted network smaller veins supply larger ones, so that the veins have different sizes. The variation in intersection probability for veins of different sizes varies with their size and distance (Fig. 5). The estimation of the intersection probability for a rooted network also depends on its structure. It is assumed here that a pair of veins supply a second vein, and that a pair of the second veins supply a third vein and so on. The number of veins is then given by $\mathcal{N} = 2^{n-1}$. Other networks where three or more veins supply a subsequent vein, and systems where a dyke is supplied by several subsystems, are also possible. The network adopted here serves to demonstrate the basic features. If the length of veins is $2r$ and their half-width h, then the mean flow rate of a vein is given by (Kay & Nedderman, 1974)

$$u = 2rah^2, \quad a = \frac{\Delta P}{3\eta \Delta L} \tag{12}$$

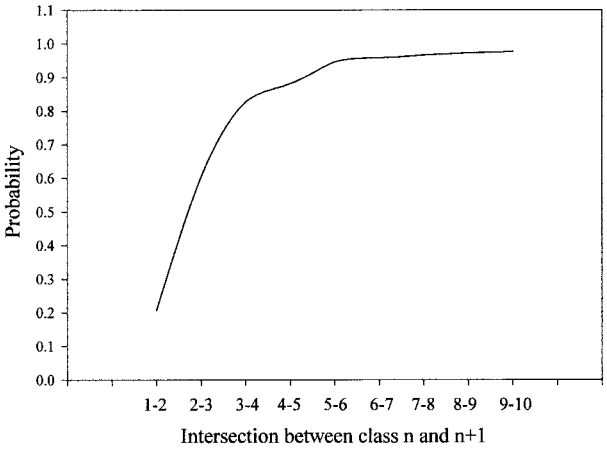

Fig. 11. The number of veins increases with decreasing vein size in a rooted system. It is assumed here that the number of veins increases with 2^{n-1} with decreasing size as given by equation (13). The diagram shows the probability of intersection between the classes of veins with exponents n and $n + 1$ for a rooted system. As an example, the intersection probability between 2^{3-1} and 2^{4-1} veins is 0·83 and is given by the ordinate of the curve at 3–4 in the diagram. The number of veins increases from 1–2 to 9–10 so that the intersection probablity also increases from 1–2 to 9–10.

where $\Delta P/\Delta L = 30$ bar/km. For a constant total flow, U, in the veins the product of their number and their volumetric flow rate must be constant and equal to U. The cross-sectional area of an ellipsoid is given by πrh. If the veins on average intersect at $\frac{1}{2}r$ then the cross-sectional area at the intersection is $\frac{3}{4}\pi rh$. If $h = \beta r$, the vein radii can be estimated from

$$U = (3/4)\pi\alpha\beta^3(2^{n-1}r_n 4). \tag{13}$$

Hence, the radii are given by

$$r_n = \left(\frac{4U}{2^{n-1}3\pi\alpha\beta^3}\right)^{1/4}. \tag{14}$$

A rooted network with 10 sets of vein sizes is considered here, that is, $n = 10$. The actual number of veins is estimated from the volume fraction of melt in the interstices and the size of a reference volume of the residuum. During the initial melting the veins must be small and a 10 m cube is therefore chosen at first as a reference volume. If the volume of a single set of veins, with n varying from one to 10, is V, and the total volume of melt in the veins in the reference volume is W, the number of veins with a given size is given by $2^{n-1}W/V$. The intersection probability for 1% melt in the veins in a 10 m cube is shown in Fig. 11. The probability is ~0·9 between the different vein sizes, except for the largest veins, and the probability of connectivity between all 10 sizes of veins is rather high, $R = 0{\cdot}075$. A rooted and connected network of veins is therefore possible during the initial stages of

melting. For this relatively small system, with a volume of 10^3 m^3, the average distances between the veins range from 10 to 80 cm with increasing vein size. The smallest veins are therefore diffusively connected and exchange components with the surrounding residuum.

For a cube of 1 km^3 dimension the widths of the conductive channels range from 2 to 4 m from the smallest to the largest, respectively, and they should be called dykes rather than veins. The distances between the dykes range from 10 to 80 m from the smallest to the largest, so that the distances between the dykes are so large that diffusive exchange with the residuum is insignificant. With increasing size their number decreases from $1{\cdot}25 \times 10^5$ to $2{\cdot}5 \times 10^2$. The probability curve for this network is identical to that of the smaller system just considered (Fig. 11).

PERMEABILITY OF A VEINED SOURCE

An estimate of the permeability of a rooted system depends on its structure, and various systems are possible. Here the permeability is estimated for a simple system with arbitrarily oriented and connected veins. The effective permeability of a non-rooted veined source is estimated using the equation for flow between parallel walls; the mean flow rate has been given by Kay & Nedderman (1974):

$$u = \frac{\Delta P h^2}{3\eta \Delta L} \qquad (15)$$

where $\Delta P/\Delta L$ is the pressure gradient due to gravity, h is the half-width of the vein, and η is the viscosity. If g is the volume fraction of melt in the veins and the reference volume is 10^6 cm^3, the volume of each of N veins with the same radius is given by

$$\nu = \frac{g10^6}{N}. \qquad (16)$$

The half-width h can then be estimated for an elliptic cross-section using (6). By using (2), (15) and (16) the permeability of a veined source can then be estimated as a function of the size of the veins and the fraction of melt present:

$$k = \frac{\pi R N r h^3}{4 \times 10^4} \qquad (17)$$

where N and R are given by (7) and (9), respectively. This equation takes the vein intersections at $\frac{1}{2}r$, so that the cross-sectional area at the intersection is $\frac{3}{4}\pi rh$. The factor 10^4 arises because the flux $\tilde{J}$ in (2) is per 1 cm^2, and the unit volume considered is 1 m^3. The permeabilitites obtained from equation (17) are similar to those obtained by Gueguen & Dienes [1989, equation (2)], who used a somewhat different approach. For 1% melt in the veins the permeability varies from 10^{-7} to 10^{-5} cm^2 when the radius of the veins decreases from 50 to 10 cm (Fig. 12). The estimated permeabilities for 1% melt are 3–5 orders of magnitude larger than the permeability, 10^{-10} cm^2, estimated for percolation from experimental analogues and theoretical considerations (Maaløe & Scheie, 1982; von Bargen & Waff, 1986; Richardson & McKenzie, 1994). The presence of veins therefore increases the permeability substantially. For a rooted network the increase in permeability may be even larger (Hart, 1993).

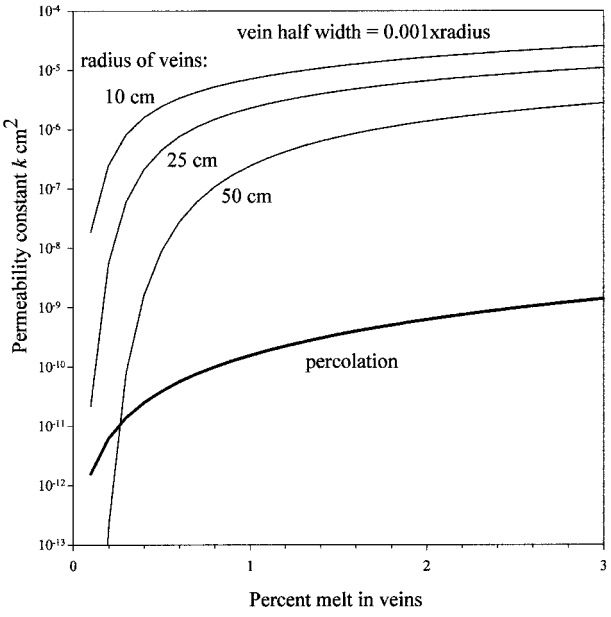

Fig. 12. The permeability constant k for a veined source as a function of percent melt in veins for different constant radii of the veins. The permeability constant increases rapidly with the percentage of melt present in the veins until ~2% melt. The permeability constant decreases with increasing radius, because the number of veins decreases with increasing radii. The permeability constant for percolation was estimated by using equations (1) and (2). When the permeability of a veined source becomes larger than the permeability for percolation, the permeability becomes controlled by the veins.

Considering the period of time for melt accumulation in the mantle, it is the mean flow rate in the veins that is important. The flow rate of the melt in the veins increases from about 10 to 60 m/a, when the percentage of melt in the veins increases from 0·5% to 1%. For a flow rate of 50 m/a the melt can ascend 50 km within a period of time of 1 kyr, which is less than the half-life of ^{226}Ra, i.e. 1·6 kyr. Considering the flow rate alone, it is therefore possible that flow in veins can account for the observed isotopic disequilibria as suggested by Richardson & McKenzie (1994). If the veins form a rooted system with an increasing vein width

with height above the onset of partial melting, then an ascent period of time of 1 kyr is actually too long.

VEIN FORMATION

The formation of a vein is preceded by the formation of a fracture. A fracture forms when the pressure of the melt exceeds a critical value given by the fracture toughness (Geertsma & de Klerk, 1969; Spence *et al.*, 1987). A satisfactory explanation for vein formation should involve an approximate estimate of the fracture toughness of partially molten lherzolite as function of overpressure and time. Such an estimate is not available and the following modelling is therefore speculative.

For the melt to form a vein the melt must exert a pressure on the grains surrounding the vein. Such a pressure can arise because the force on a grain with a free grain–melt surface is larger than the force on grains surrounded only by an interstitial melt. The equilibrium shape of the grains within peridotite is like a β-tetrakaidecahedron when the grains have the same size (Williams, 1968). The principle is demonstrated here using grains with a simple cubic shape as shown in Fig. 13a. The cubic grains have interstitial melt at their corners. The shape of the interstices at a single cube corner is taken to be pseudo-tetrahedral, the three corner sides differing in side length from the sides of the triangular base. The grains with a free surface are exposed to a force given by the pressure multiplied by the area. Let the side of a grain be one unit length and the overpressure ΔP; the force is then $F = 1 \times \Delta P$. Let h be the height of the melt corner in the side units and V the volume fraction of melt; then $h = 3\sqrt{2}\,V/8$. The area of the cube side with melt at the four corners is then $a = 1 - 6h^2$. For 1% melt $h = 0{\cdot}0053$ and $a = 0{\cdot}9998$, so that the reduction in side area is negligible. The force on the A-type cube is $(1 - 6h^2)\Delta P = 0{\cdot}9998\Delta P$. The grains along the vein are exposed to this force, which may cause extension of the initial vein. The grains to the right of the A-cube, referred to here as the B-cubes, are compressed by the melt situated at their eight corners and do not by themselves exert a force on the surrounding grains. According to this model the condition for vein initiation is that some grains attain a free surface towards the melt, so that these grains form the nuclei for vein formation.

During melting the increasing volume of the melt increases the pressure of the interstitial melt. The increase in pressure depends on the melting rate and the creep rate of the residuum. The creep rate is determined based on how the entire partially molten region increases in volume, which is difficult to estimate. An estimate of the maximal increase in the pressure of the interstitial melt may be obtained by considering the pressure increase of the melt within a slab with a permeable and stiff matrix with parallel veins on each side. The variation in overpressure was estimated for a melt viscosity of 10 poise, a melt generation rate of $3{\cdot}6 \times 10^{-7}$ a^{-1}, a compressibility of 2×10^{-6} bar^{-1} (Scarfe *et al.*, 1979), and a permeability constant equal to 10^{-10} cm^2, by using the permeability version of the heat source equation of Carslaw & Jaeger [1973, equation (3.14.7)]. The equations for permeable flow and heat flow are both solutions to the same differential Laplace equation, the only difference being the constants involved. The solutions obtained for heat flow can therefore also be applied for permeable flow, with the appropriate changes in constants. In applying this equation the volume of the melting solid should be subtracted from the volume of the melt generated. For a 1 m wide slab of the residuum, the maximum

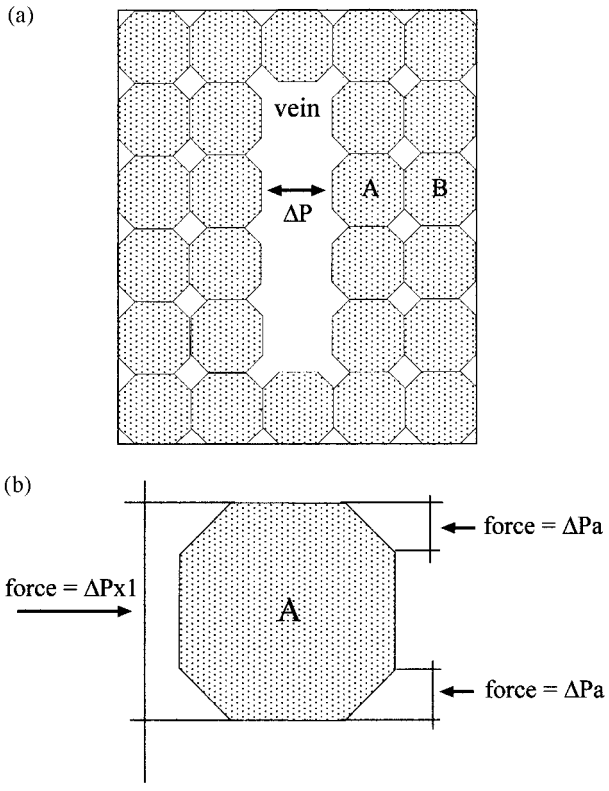

Fig. 13. Illustration of the pressure relations of cubic grains with a free surface towards the melt in a vein. The overpressure of the melt is given by ΔP. (a) The position of the grains around a vein. Grain A has a free surface towards the melt in the vein. Grain B is surrounded by other grains on all six sides. The melt at the eight corners of grain B exerts pressure on grain B, but these form opposite pairs that cancel out. (b) The difference in the forces on the two sides of grain A. The area given by a is the projection of the triangular corner onto the plane shown. The force on the left side is $\Delta P \times$ (unit area). The opposite force on the right side is much less, $4\Delta Pa$. For 1% melt the resulting force on the A-type cube is $0{\cdot}9998\Delta P$, the side of the cube being one length unit.

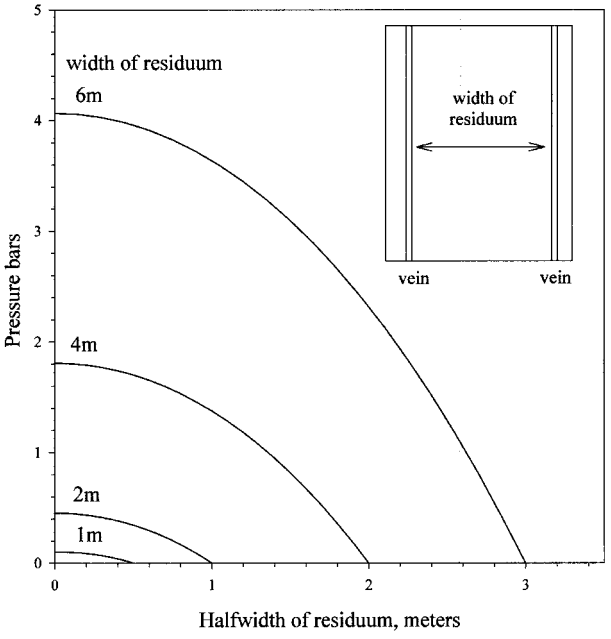

Fig. 14. The overpressure arising by melting in a permeable and stiff slab of a residuum as a function of slab half-widths between 0·5 and 3 m. The inset show the slab of residuum situated between two parallel veins. This estimate neglects the creep of the residuum, which will result in smaller overpressures. Nevertheless, the overpressures for a stiff residuum suggest that the overpressure probably is at least a fraction of a bar for a residuum undergoing creep.

overpressure is 0·11 bar, and 4 bars for a 6 m wide slab. The maximum overpressure of the melt in the matrix increases with the square of the width of the matrix, as is evident from Fig. 14. These overpressures arise entirely as a result of the volume expansion caused by the melting. The equation used assumes that the solid is stiff without any creep. The residuum, however, deforms by creep, so that the estimated pressures shown in Fig. 14 are the maximum possible values. However, the relatively large overpressures estimated for stiff slabs of a few metres width suggest that it is possible that vein formation can take place entirely as a result of the overpressure caused by the volume expansion arising by melting. As shown below, the overpressures for vein formation by creep deformation are small.

The viscous deformation of an elliptic crack with an internal overpressure can be estimated using the creep rate equation for peridotite of Hirth & Kohlstedt (1995) and the viscous deformation equations for an elliptic cross-section (Maaløe, 2002). At 1823 K the creep rate is $3 \times 10^{-12}\,s^{-1}$, equivalent to a viscosity of $1{\cdot}1 \times 10^{-17}$ poise. A 1 cm long crack initially has an annual increase in volume of $2 \times 10^{-6}\,cm^3/a$ for an internal overpressure of only 5×10^{-3} bar. This volume equals the annual increase in the fraction of melt within 1 cm of the crack. The small overpressure of the melt needed to expand the crack suggests that veins may form as a result of the overpressure of the melt.

DISCUSSION

The observed isotope activity ratios can be achieved only if melt extraction begins to occur when the residuum contains $< 1\%$ melt. It is evident from the modelling presented here based on random oriented ellipsoidal veins that vein connectivity begins to occur at a similar percentage. Some melt must also be present in the interstices of the residuum, so that the results of this study suggest that the total amount of melt should be slightly larger than 1% for connectivity and efficient melt extraction. Vein connectivity within the range of 0·1–0·5% melting would have been a preferable result. However, when considering the approximation involved concerning the planar shape of the veins, the small uncertainty in the estimated ranges of melt percentages is considered acceptable.

During the earliest stages of melting, the melt in the veins has the same composition as the interstitial melt in the residuum. With larger degrees of critical melting the composition of the melt in the veins differs from that of the residuum and the effect of diffusion must be taken into account. The diffusion distance from a vein depends on the interstitial migration rate within the residuum and therefore on the permeability. For permeability constants larger than $10^{-10}\,cm^2$ the flow rate of melt in the interstices is sufficiently large that steady-state diffusion will not change the bulk composition of the residuum significantly over a distance of more than a few decimetres. Available estimates of the permeability of the residuum suggest that permeabilities of this order of magnitude are realistic.

Ascending melts that are generated by critical melting will have a higher temperature than the partially molten peridotite surrounding the veins (Maaløe, 2003). As the veins constitute a minor fraction of the total volume, the melt must largely attain the same temperature as the residuum. The melts must therefore react with the peridotite adjacent to the walls of the veins, which changes the major and trace element compositions of the ascending melts. The first ascending melts must change their compositions. If the flow rate of the melt becomes constant, then a steady state arises, so that the concentration gradients in the residuum become constant (Fig. 10). The compositions and the activity ratios of the melts then become determined mainly by the addition of interstitial melt from the residuum. The major part of the incompatible elements enters the melt at low degrees of melting, so that later additions of melt decrease the concentrations of these elements, but hardly change their concentration ratios.

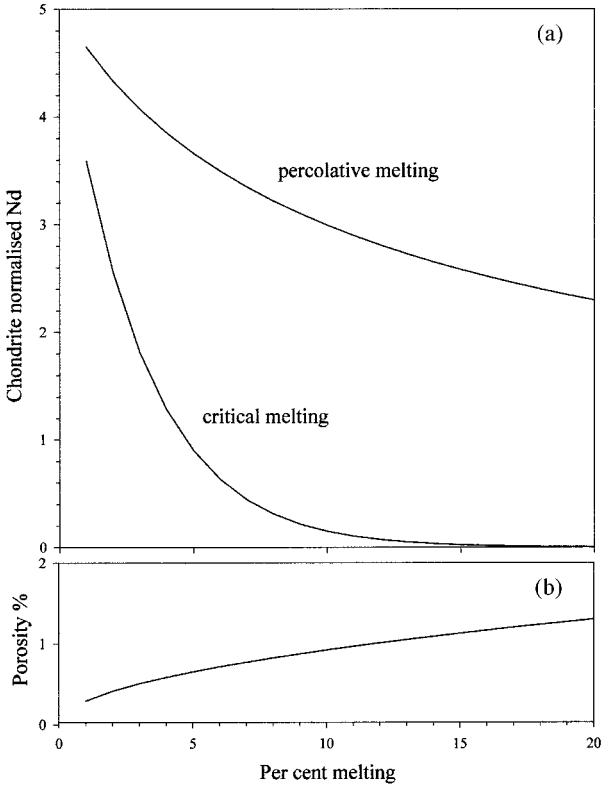

Fig. 15. (a) The chondrite-normalized values for Nd in residua formed during percolative and critical melting. The bulk distribution coefficient for Nd was estimated as 0·0192, and the normalized ratio of the source as three (Maaløe & Pedersen, 2003). The estimate for percolative melting was made for a mantle ascent rate of 10 cm/a, and an increase in the melt fraction of 5×10^{-8} cm^{-1}, using equation (1) to estimate the permeability. The percolation begins when the first melt is generated. The critical melting curve was estimated assuming 1% melt in the residuum. The Nd values at 1% melting differ because percolation starts at <1% melting. The calculation methods of Maaløe & Johnston [1986, equation (17)] and Spiegelman & Elliot (1993) were used. (b) The increase in porosity as a function of percentage melting by percolative melting.

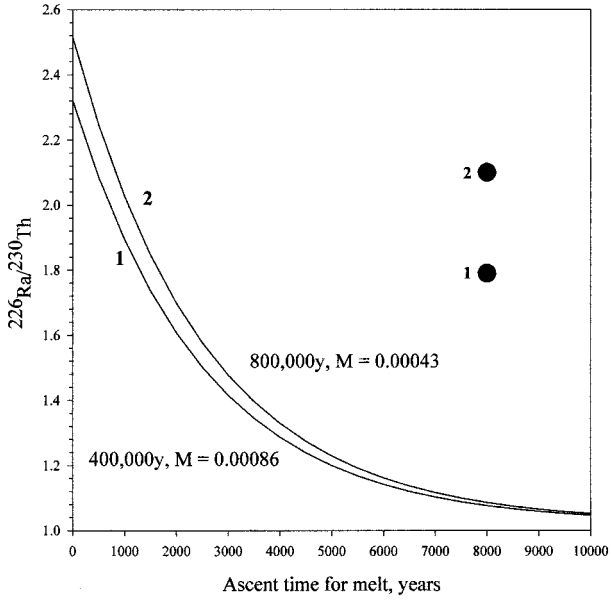

Fig. 16. Variation of average (^{226}Ra/^{230}Th) in the melts as a function of maximum ascent time for the melts. The source is a garnet lherzolite with bulk $D_U = 0{\cdot}00583$ and $D_{Th} = 0{\cdot}00353$ (Zou & Zindler, 2000). Curves 1 and 2 are for 20% partial melting by volume of the mantle in 400 and 800 kyr, respectively. The ages of the residual melts therefore vary from 0 a to either 400 ka or 800 ka. The M values are averages in the units kg/a m^3. The curves are compared with the average values of the residual melts (filled circles 1 and 2) estimated using equations (27) and (28) of Zou & Zindler (2000). These average values do not take into account the radioactive decay during ascent.

As both critical and percolative melting can result in the same activity ratios, other approaches must be used to evaluate of the melting mode. Critical melting continuously extracts incompatible elements from the residuum, whereas percolative melting both adds and extracts these elements. Melt is extracted from a unit volume, but at the same time melt with a slightly higher concentration of incompatible elements is added by the melt ascending from below. The extraction of incompatible elements from the residuum is therefore less intense for percolative melting than for critical melting. The ratios of chondrite-normalized rare earth elements in the residual harzburgite may therefore provide an indication of the melting mode for the petrogenesis of tholeiitic basalts. The normalized rare earth element concentrations of harzburgite attain values of ~0·1 between La and Lu, the pattern being fairly flat (Frey, 1984). The variation in normalized Nd for residua with degree of melting is shown in Fig. 15. It is evident that the values for Nd for percolation are >0·1, whereas the values for critical melting are ~0·1. As harzburgite is likely to be the final residuum in equilibrium with abyssal tholeiites, this evidence suggests that the melting mode at some stage must change from a percolative one to a critical one.

Estimates of (^{226}Ra/^{230}Th) for basalts generated by critical melting generally assume that the ascent of melt within the partially molten zone occurs instantaneously. The activity ratios of basalts are assumed to reflect the average ratio of all the melt fractions generated within a melting column in the ascending mantle (McKenzie, 1985; Williams & Gill, 1989; Zou & Zindler, 2000). The melts extracted at the lowest degrees of partial melting have the largest activity ratios; however, they should also have ascended for the longest distance, and therefore the longest periods of time. The isotope ^{226}Ra can therefore undergo a significant amount of decay. The variation in the (^{226}Ra/^{230}Th) of the extracted melts for two mantle ascent models is shown in Fig. 16. Both models

assume the porosity is 0·2%, and that a constant fraction of the solid residuum melts within a year. The models assume 20% melting within 400 kyr and 800 kyr, respectively. The calculation of the variation in the activity ratio of the melt is shown in the Appendix. The period of time for the ascent of the melt is defined as the time it takes for the first extracted melt to ascend to the top of the melting column. It is evident that the period of time for melt ascent cannot be ignored. There is a marked decrease in $(^{226}Ra/^{230}Th)$ with the duration of the ascent. The $(^{226}Ra/^{230}Th)$ observed for abyssal tholeiites shows scatter within the range 1·1–4·6; most values are within 1·5–2·5 (Spiegelman & Elliot, 1993; Richardson & McKenzie, 1994; Sims *et al*., 2003). It is evident, therefore, that the period of time for melt ascent within the partially molten zone typically is less than ∼3 kyr.

The relatively large scatter in $(^{226}Ra/^{230}Th)$ for abyssal tholeiites may be related either to variations in the ascent rates of the melts from their source regions, or to various storage times in an abyssal magma chamber. It was shown by Sims *et al*. (2003) that $(^{226}Ra/^{230}Th)$ is negatively correlated with $(^{230}Th/^{238}U)$ in abyssal tholeiites from the East Pacific Rise. The $(^{226}Ra/^{230}Th)$ ratio decreases from four to one while the $(^{230}Th/^{238}U)$ ratio increases from 1 to 1·26. Sims *et al*. concluded that melts with $(^{230}Th/^{238}U)$ ratios of ∼1·0 were generated within the spinel lherzolite field, and those with large ratios were generated within the garnet lherzolite field. If variations in the storage time in an abyssal magma chamber are controlling the activity ratios then $(^{226}Ra/^{230}Th)$ is not expected to correlate with $(^{230}Th/^{238}U)$. The abyssal tholeiites from the East Pacific Rise with $(^{230}Th/^{238}U)$ of ∼1·3 have $(^{226}Ra/^{230}Th)$ of ∼1·0, and are also the most fractionated basalts of the trend (Sims *et al*., 2003). A $(^{230}Th/^{238}U)$ ratio of ∼1·3 indicates generation within the garnet lherzolite field, because generation within the spinel lherzolite field result in ratios $<1·0$ (Zou & Zindler, 2000). The melts ascending from the garnet lherzolite field have a longer ascent path than those from the spinel lherzolite field, which could result in a longer period of time for ascent and more extensive fractionation, as suggested by Sims *et al*. (2003). Alternatively, the ascent of melt within partially molten garnet lherzolite could be slower than within partially molten spinel lherzolite, although it is not obvious why this should be the case. The large $(^{226}Ra/^{230}Th)$ ratios of the melts equilibrated within the spinel lherzolite zone suggest that their ascent within the partial melting zone must have been faster than by percolative flow, and therefore that melt ascent may have taken place in veins.

The critical melting model implies that veins are formed in the residuum. The dynamics of eruptions and sub-volcanic intrusions also appear to require the formation of a veined source region within the mantle. The intrusions of batches of magma into subvolcanic and abyssal magma chambers show that these intrusions must be preceded by magma accumulation in a source region situated within the upwelling mantle. The melt can leave such a source region only if the mantle surrounding the source region exerts a pressure on the source region, the pressure being caused by the buoyancy of the melt. The source region must undergo compaction as the magma leaves the source region. It can be shown that this compaction occurs by elastic deformation rather than by plastic deformation Maaløe, 2003), and that the melt in the source region not is an interstitial melt, but rather that it is situated in veins. A veined model for the partially molten mantle is therefore consistent with both the deformational behaviour of a mantle source region and the critical melting model. The formation of veins or layers of melt is also suggested by the central focusing of the magmas ascending beneath mid-ocean ridges. Taking the degree of melting for primary abyssal tholeiite as 20% and the thickness of the oceanic crust as 7 km, then the partially molten zone of the ascending mantle must be at least 70 km wide, if the ascent rate of the mantle equals the spreading rate. The widths of the neovolcanic rift zones are not more than 3–5 km (MacDonald, 1982), so that the melt must become focused towards the rift zones. Some of the focusing may be related to the necking of the upwelling mantle (Ceuleneer, 1991; Su & Buck, 1993). The focusing of the ascending melt may be related to an increasing ascent rate of the upwelling mantle towards its central axis. Such an increase in ascent rate causes shear, which tilts the veins away from the ridge axis so that the ascending melt becomes focused towards the centre of the upwelling (Maaløe, 1998).

The accumulation of melt in the mantle must take place at degrees of melting less than that necessary for the bulk production of basaltic magmas. Melilitites are alkaline mafic magmas considered to be generated by the lowest degrees of mantle melting, estimated at 4–6% melting by Maaløe *et al*. (1992). The method applied for this estimate assumes batch melting and is independent of the source concentrations. However, an exact estimate depends on the accuracy on the distribution coefficients used. In comparison, the degree of melting required to generate alkali olivine basalt has been estimated at 11–12% by Clague & Frey (1982) and Maaløe & Pedersen (2003), whereas Sims *et al*. (1999) suggested only 3%. These percentages are consistent with initial melt accumulation of 1% or less.

This study has considered the initial formation of veins, where the veins are stationary. When the veins becomes larger and form a network with a certain vertical extension, then it is possible that they start to propagate upwards. The reason for considering this possibility is that a connected vertical network of veins will result in excessive overpressures within the mantle source region (Maaløe, 1999). There may, therefore, be a transition from a stationary network of veins at great depths to a system of intruding dykes at shallower depths. A similar model has previously been suggested by Shaw (1980).

CONCLUSIONS

The earliest stages of melting of the mantle must occur by batch melting. After the residuum becomes permeable the melting mode changes to reactive percolative melting. Thereafter veins may begin to form. If the distances between the early formed veins are less than a few decimetres, then melting will continue to be reactive. If the distances between the veins increase gradually with increasing degree of melting, then there is a transition from reactive melting to critical melting. The degree of melting at which this transition occurs has yet to be determined. The results presented here suggest that vein connectivity is possible in the presence of $\sim$1% melt, so that melting could become critical soon after the onset of permeability.

Both the critical melting model and a percolative model including veins can account for the activity ratios observed for MORB. These two melting models should therefore be evaluated using a combination of activity ratios and trace elements. The critical melting model can be applied if the melt extraction takes place in the presence of $<1\%$ melt in the residuum. The results of this study suggest that if randomly oriented veins form in the partially molten mantle then this condition can be fulfilled. The limited material exchange between the accumulated melt in the veins and the residuum required by the critical melting model constrains the migration rate of the interstitial melt. For permeability constants of about or larger than $10^{-10}\,\mathrm{cm}^2$ the melt migration rate in the residuum is sufficiently fast for insignificant material exchange. The critical melting model appears possible, especially if the veins form a rooted network, as suggested by Hart (1993). It is tentatively suggested that vein formation can occur by the overpressure caused by the volume expansion during melting. The melts ascending in veins within the partially molten mantle can undergo a significant decrease in $(^{226}\mathrm{Ra}/^{230}\mathrm{Th})$, which should be taken into account when evaluating these activity ratios for basalts.

ACKNOWLEDGEMENTS

The author thanks G. Ceuleneer, K. W. W. Sims, B. D. Marsh and M. Wilson for constructive and helpful reviews, which have improved the manuscript substantially. This study is part of the SUBMAR project supported by NFR, the Norwegian Research Council.

REFERENCES

Amundsen, H. E. F., Griffin, W. L. & O'Reilly, S. Y. (1988). The nature of the lithosphere beneath northwestern Spitsbergen: xenolith evidence. *Norwegian Geological Survey Special Publication* **3**, 58–65.

Batanova, V. G. & Sobolev, A. V. (2000). Compositional heterogeneity in subduction-related mantle peridotites, Troodos massif, Cyprus. *Geology* **28**, 55–58.

Batanova, V. G., Suhr, G. & Sobolev, A. V. (1998). Origin of geochemical heterogeneity in the mantle peridotites from the Bay of Islands ophiolite, Newfoundland, Canada: ion microprobe study of clinopyroxenes. *Geochimica et Cosmochimica Acta* **62**, 853–866.

Bodinier, J., Guiraud, M., Fabriès, J., Dostal, J. & Dupuy, C. (1987). Petrogenesis of layered pyroxenites from the Lherz, Freychinède and Prades ultramafic bodies (Ariège, French Pyrénées). *Geochimica et Cosmochimica Acta* **51**, 279–290.

Bodinier, J. L., Vasseur, G., Vernieres, J., Dupuy, C. & Fabries, J. (1990). Mechanisms of mantle metasomatism: geochemical evidence from the orogenic peridotite. *Journal of Petrology* **31**, 597–628.

Boudier, F. (1978) Structure and petrology of the Lanzo peridotite massif (Piedmont Alps). *Geological Society of America Bulletin* **89**, 1574–1591.

Boyd, F. R. & McCallister, R. H. (1976). Densities of fertile and sterile garnet peridotites. *Geophysical Research Letters* **3**, 509–512.

Carslaw, H. S. & Jaeger, J. C. (1973). *Conduction of Heat in Solids*. Oxford: Clarendon Press, 510 pp.

Ceuleneer, G. (1991). Evidence for a palaeo-spreading center in the Oman ophiolite: mantle structures in the Maqsad area. In: Peters, T. (ed.) *Ophiolite Genesis and Evolution of the Oceanic Lithosphere*. Dordrecht, Ministry of Petroleum and Minerals, Sultanate of Oman, pp. 147–173.

Ceuleneer, G. & Rabinowicz, M. (1992). Mantle flow and melt migration beneath oceanic ridges: models derived from observations in ophiolites. In: Peters, T. J., Nicolas, A. & Coleman, R. G. (eds) *Ophiolite Genesis and Evolution of the Oceanic Crust. Geophysical Monograph, American Geophysical Union* **71**, 123–153.

Ceuleneer, G., Monnereau, M., Rabinovicz, M. & Rosemberg, C. (1993). Thermal and petrological consequences of melt migration within mantle plumes. *Philosophical Transactions of the Royal Society of London, Series A* **342**, 53–64.

Chalmers, B. (1964). *Principles of Solidification*. New York: John Wiley, 319 pp.

Clague, D. A. & Frey, F. A. (1982). Petrology and trace element geochemistry of the Honolulu volcanics, Oahu: implications of the oceanic mantle beneath Hawaii. *Journal of Petrology* **23**, 447–504.

Conquéré, F. (1977). Petrologie des pyroxénites litées dans les complexes ultramafiques de l'Ariège (France) et autre gisements de lherzolite à spinelle, I. Compositions minéralogiques et chimiques, évolution des conditions d'équilibre des pyroxénites. *Bulletin de la Société Française de Minéralogie et de la Cristallographie* **100**, 42–137.

Cortini, M. (1990). Fractal magmatic systems. *Nature* **346**, 226.

Dikey, J. S., Jr (1970). Partial fusion products in alpine type peridotites: Serrania de la Ronda and other examples. *Mineralogical Society of America, Special Paper* **3**, 3–49.

Frey, F. A. (1984). Rare earth element abundances in the upper mantle. In: Henderson, P. (ed.) *Rare Earth Element Geochemistry*. Amsterdam: Elsevier, pp. 153–203.

Geertsma, J. & de Klerk, F. (1969). A rapid method of predicting width and extent of hydraulically induced fractures. *Journal of Petroleum Technologies* **21**, 1571–1581.

Gueguen, Y. & Dienes, J. (1989). Transport properties of rocks from statistics and percolation. *Mathematical Geology* **21**, 1–13.

Hart, S. R. (1993). Equilibration during mantle melting: a fractal tree model. *Proceedings of the National Academy of Sciences of the USA* **90**, 11914–11918.

Hellebrand, E., Snow, J. E., Dick, H. J. B. & Hofmann, A. W. (2001). Coupled major and trace elements as indicators of the extent of melting in mid-ocean-ridge peridotites. *Nature* **410**, 677–681.

Hestir, K. & Long, J. C. S. (1990). Analytical expressions for the permeability of random two-dimensional Poisson fracture networks based on regular lattice percolation and equivalent media theories. *Journal of Geophysical Research* **95**, 21565–21581.

Hirth, G. & Kohlstedt, D. L. (1995). Experimental constraints on the dynamics of partially molten upper mantle: deformation in the diffusion regime. *Journal of Geophysical Research* **100**, 1981–2000.

Hofmann, A. W. (1980). Diffusion in natural silicate melts: a critical review. In: Hargraves, R. B. (ed.) *Physics of Magmatic Processes*. Princeton, NJ: Princeton University Press, pp. 385–417.

Ivanowich, M. (1982). The phenomena of radioactivity. In: Ivanovich, M. & Harmon, R. S. (eds) *Uranium Series Disequilibrium: Applications to Environmental Problems*. Oxford: Clarendon Press, pp. 1–32.

Iwamori, H. (1994). ^{238}U–^{230}Th–^{226}Ra and ^{235}U–^{231}Pa disequilibria produced by mantle melting with porous flow and channel flows. *Earth and Planetary Science Letters* **125**, 1–16.

Johnson, K. T. M., Dick, H. J. B. & Shimizu, N. (1990). Melting in the upper mantle: an ion microprobe study of diopsides in abyssal peridotite. *Journal of Geophysical Research* **95**, 2662–2678.

Kay, J. M. & Nedderman, R. M. (1974). *An Introduction to Fluid Mechanics and Heat Transfer*. Cambridge: Cambridge University Press, 322 pp.

Kelemen, P. B., Hirth, G., Shimizu, N., Spiegelman, N. & Dick, H. J. B. (1997). A review of melt migration processes in the adiabatically upwelling mantle beneath oceanic spreading ridges. *Philosophical Transactions of the Royal Society of London, Series A* **355**, 1–35.

Kornprobst, J. (1969). Le massif ultrabasique des Beni Bouchera (Rif Interne, Maroc): étude des péridotites de haute température et de haute pression, et des pyroxénolites à grenat ou sans grenat, qui lui sont associées. *Contributions to Mineralogy and Petrology* **23**, 283–322.

Long, J. C. S., Remer, J. S., Wilson, C. R. & Witherspoon, P. A. (1982). Porous media equivalents for networks of discontinuous fractures. *Water Resources Research* **18**, 645–658.

Lundstrom, C. C., Gill, J., Williams, Q. & Perfit, M. R. (1995). Mantle melting and basalt extraction by equilibrium porous flow. *Science* **270**, 1958–1961.

Maaløe, S. (1982). Geochemical aspects of permeability controlled partial melting and fractional crystallization. *Geochimica et Cosmochimica Acta* **46**, 43–57.

Maaløe, S. (1998). Extraction of primary abyssal tholeiite from a stratified plume. *Journal of Geology* **106**, 163–179.

Maaløe, S. (1999). Magma accumulation in Hawaiian plume sources. *American Journal of Science* **139**, 139–156.

Maaløe, S. (2002). Physical behaviour of the plume source during intermittent eruptions of Hawaiian basalts. *Contributions to Mineralogy and Petrology* **142**, 653–665.

Maaløe, S. (2003). Basic phase relations of batch, percolative and critical melting. *Mineralogy and Petrology* **77**, 1–24.

Maaløe, S. & Johnston, A. D. (1986). Geochemical aspects of some accumulation models for primary magmas. *Contributions to Mineralogy and Petrology* **93**, 449–458.

Maaløe, S. & Pedersen, R. B. (2003). Two methods for estimating the degree of partial and trace element concentrations in the sources for primary magmas. *Chemical Geology* **193**, 155–156.

Maaløe, S. & Scheie, Å. (1982). The permeability controlled accumulation of primary magma. *Contributions to Mineralogy and Petrology* **81**, 350–357.

Maaløe, S., James, D., Smedley, P., Petersen, S. & Garmann, L. (1992). The Koloa volcanic suite of Kauai, Hawaii. *Journal of Petrology* **33**, 761–784.

MacDonald, K. C. (1982). Mid-ocean ridges: fine-scale tectonic, volcanic, and hydrothermal processes within the plate boundary zone. *Annual Review of Earth and Planetary Sciences* **10**, 155–190.

McKenzie, D. (1985). ^{230}Th–^{238}U disequilibrium and the melting processes benath ridge axes. *Earth and Planetary Science Letters* **72**, 149–157.

McKenzie, D. & Bickle, M. J. (1988). The volume and composition of melt generated by extension of the lithosphere. *Journal of Petrology* **29**, 625–679.

Obata, M. & Nagahara, N. (1987). Layering of alpine-type peridotite and the segregation of partial melt in the upper mantle. *Journal of Geophysical Research* **92**, 3467–3474.

Python, M. & Ceuleneer, G. (2003). Nature and distribution of mafic dikes in the mantle section of the Oman ophiolite. *G*^{3} (in press).

Quick, J. (1981). Petrology and petrogenesis of the Trinity peridodite, an upper mantle diapir in the eastern Klamath mountains, Northern California. *Journal of Geophysical Research* **86**, 11837–11863.

Richardson, C. N. & McKenzie, D. (1994). Radioactive disequilibria from 2D models of melt generation by plumes and ridges. *Earth and Planetary Science Letters* **128**, 425–437.

Richardson, C. N., Lister, J. R. & McKenzie, D. (1996). Melt conduits in a viscous porous matrix. *Journal of Geophysical Research* **101**, 20423–20432.

Richet, P. & Bottinga, Y. (1986). Thermochemical properties of silicate glasses and liquids: a review. *Reviews of Geophysics* **24**, 1–25.

Robie, R. A. & Waldbaum, D. R. (1968). Thermodynamic properties of minerals and related substances at 298·15°K (25°C) and one atmosphere (1·013 bars) pressure and at high temperatures. *US Geological Survey Bulletin* **1259**, 256 pp.

Rubin, A. M. (1998). Dike ascent in partially molten rock. *Journal of Geophysical Research* **103**, 20901–20919.

Salters, V. J. M. & Longhi, J. (1999). Trace element partitioning during the initial stages of melting beneath mid-ocean ridges. *Earth and Planetary Science Letters* **166**, 15–30.

Scarfe, C. M., Mysen, B. O. & Virgo, D. (1979). Changes in viscosity and density of melts of sodium disilicate, metasilicate, and diopside composition with pressure. *Carnegie Institution of Washington Yearbook* **78**, 547–551.

Schubert, W. (1977). Reaktione im alpinotypes Peridotite-massiv von Ronda (Spanien) und seinen partiellen Schmeltzprodukten. *Contributions to Mineralogy and Petrology* **62**, 205–220.

Seyler, M., Toplis, M. J., Lorand, J.-P., Luguet, A. & Cannat, M. (2001). Clinopyroxene microtextures reveal incompletely extracted melts in abyssal peridotites. *Geology* **29**, 155–158.

Shaw, H. R. (1980). The fracture mechanisms of magma transport from the mantle to the surface. In: Hargraves, R. B. (ed.) *Physics of Magma Processes*. Princeton, NJ: Princeton University Press, pp. 201–264.

Sims, K. W., DePaolo, D. J., Murrel, M. T., Balridge, W. S., Goldstein, S., Clague, D. & Jull, D. (1999). Porosity of the melting zone and variations in the solid mantle upwelling rate beneath Hawaii: inferences fromn ^{238}U–^{230}Th–^{226}Ra and ^{235}U–^{281}Pa disequilibria. *Geochimica et Cosmochimica Acta* **63**, 4119–4138.

Sims, K. W., Goldstein, S. J., Blichert-Toft, J., Perfit, M. R., Kelemen, P., Fornari, D. J., Michael, P., Murrell, M. T., Hart, S. R., DePaolo, D. J., Layne, G., Ball, L., Jull, M. & Bender, J. (2003). Chemical and isotopic constraints on the generation and transport of magma beneath the East Pacific Rise. *Geochimica et Cosmochimica Acta* **66**, 3481–3504.

Sleep, N. H. (1988). Tapping melts by veins and dikes. *Journal of Geophysical Research* **93**, 10255–10272.

Sobolev, A. V. & Shimizu, N. (1993). Ultra-depleted primary melt included in an olivine from the Mid-Atlantic ridge. *Nature* **363**, 151–153.

Spence, D. A., Sharp, P. W. & Turcotte, D. L. (1987). Buoyancy-driven crack propagation: a mechanism for magma migration. *Journal of Fluid Mechanics* **174**, 135–153.

Spiegelman, M. & Elliot, T. (1993). Consequences of melt transport for uranium series disequilibrium in young lavas. *Earth and Planetary Science Letters* **118**, 1–20.

Stevenson, D. J. (1989). Spontaneous small-scale melt segregation in partial melts undergoing deformation. *Geophysical Research Letters* **16**, 1067–1070.

Su, W. & Buck, W. R. (1993). Buoyancy effects on mantle flow under mid-ocean ridges. *Journal of Geophysical Research* **98**, 12191–12205.

Takazawa, E., Frey, F. A., Shimizu, N. & Obata, M. (2000). Whole rock compositional variations in an upper mantle peridotite (Horoman, Hokkaido, Japan): are they consistent with a partial melting process? *Geochimica et Cosmochimica Acta* **64**, 695–716.

von Bargen, N. & Waff, H. S. (1986). Permeabilities, interfacial areas and curvatures of partially molten systems: results of numerical computations of equilibrium microstructures. *Journal of Geophysical Research* **91**, 9261–9276.

Walter, M. J. (1998). Melting of garnet peridotite and the origin of komatiite and depleted lithosphere. *Journal of Petrology* **39**, 29–60.

Williams, R. E. (1968). Space-filling polyhedron: its relation to aggregates of soap bubbles, plant cells, and metal crystallites. *Science* **161**, 276–277.

Williams, R. W. & Gill, J. B. (1989). Effects of partial melting on the uranium decay series. *Geochimica et Cosmochimica Acta* **53**, 1607–1619.

Wilshire, H. G. & Kirby, S. H. (1989). Dikes, joints, and faults in the upper mantle. *Tectonophysics* **161**, 23–31.

Wood, D. A. (1979). A variably veined suboceanic upper mantle—genetic significance for mid-ocean ridge basalts from geochemical evidence. *Geology* **7**, 499–503.

Zou, H. & Zindler, A. (2000). Theoretical studies of ^{238}U–^{230}Th–^{226}Ra and ^{235}U–^{231}Pa disequilibria in young lavas produced by mantle melting. *Geochimica et Cosmochimica Acta* **64**, 1809–1817.

APPENDIX

Various dynamic melting models have been proposed. The melting model used here is therefore described in detail. Let partial melting begin at depth $z_0 = 0$ and at time t_0. Further, let the mantle become permeable when the interstitial melt volume becomes φ at depth z_c and at time t_c. Melt extraction begins at this stage and continues until depth z_e and time t_e. The melts extracted between depth z_c and z_e ascend and become mixed together. The melt extracted from the residuum at any given depth z_i has an initial activity ratio R_i, which is the activity ratio of the melt in the residuum. During subsequent ascent the radiogenic isotopes in the melt undergo decay so that the activity ratios decrease. When the melt reaches height z_e the activity ratio R_i has decreased to R_e. The activity ratio of all the melts accumulated at z_e is then estimated from their initial activity ratios and the time it takes for the melts to ascend from depth z_i to z_e. Most critical or dynamic melting models estimate instead the activity ratio of the accumulated melt from an average of R_i, but this ignores the decay during ascent. Subsequently, the volume of the extracted melt is estimated, and the equations for the accumulated extracted melt are then derived.

The variation in the activity ratio (^{226}Ra/^{230}Th) during ascent is estimated using the critical melting equations [(8), (9) and (10)] given by Zou & Zindler (2000) for the (^{226}Ra) and (^{230}Th) activities of the interstitial melt in the residuum. These equations are derived with the assumption that the residuum is not in diffusive exchange with the ascending melt. The ascending melt accumulates melt from the residuum during its ascent, so that the activity of the accumulated melt depends on the volume of melt received from the residuum, the initial activity ratio of this melt, and its ascent rate.

Melt accumulation begins at a critical volume of the interstitial melt given by φ. Let the unit volume of the residuum be 1 cm^3 and let the total volume of the unit volume being melted be ΔS cm^3. Let the densities of the solid and melt be $\rho_s = 3{\cdot}3$ g/cm^3 and $\rho_f = 3{\cdot}0$ g/cm^3. The volume of the melt generated is then $\Delta S\rho_s/\rho_f$. The volume of the total residuum, R, is estimated from

$$R = (1 - \Delta S) + \varphi R \tag{A1}$$

so that

$$R = \frac{1 - \Delta S}{1 - \varphi}. \tag{A2}$$

The volume of all the melt generated is $\Delta S\rho_s/\rho_f$. At the critical degree of melting this volume equals the interstitial volume so that

$$\frac{\Delta S(\rho_s/\rho_f)}{R} = \varphi. \tag{A3}$$

The volume of solid melted, ΔS_0, at the critical degree of melting is then

$$\Delta S_0 = \frac{\varphi}{\rho_s/\rho_l + \varphi(1 - \rho_s/\rho_l)}. \quad \text{(A4)}$$

The volume of solid in the residuum at this stage is $S_0 = 1 - \Delta S_0$. The volume of the interstitial melt m_0 is

$$m_0 = \Delta S_0 \frac{\rho_s}{\rho_f}. \quad \text{(A5)}$$

The volumetric melting rate is estimated on the assumption that a constant fraction of the residuum melts within a year. Hence

$$\frac{d\Delta S}{dt} = u(1 - \Delta S) \quad \text{(A6)}$$

so that

$$\Delta S = 1 - e^{-ut}. \quad \text{(A7)}$$

The period of time between the onset of partial melting and melt extraction, t_c, is then given by

$$t_c = \frac{1}{u}\ln\left(\frac{1}{1 - \Delta S_0}\right). \quad \text{(A8)}$$

The total volume of melt generated at time t is given by

$$m = (1 - e^{-ut})\frac{\rho_s}{\rho_f}. \quad \text{(A9)}$$

The volume of extracted melt is obtained from

$$m_{ex} = m - \varphi R \quad \text{(A10)}$$

so that for $t > t_c$

$$m_{ex} = (1 - e^{-ut})\frac{\rho_s}{\rho_f}\left(\frac{\rho_s}{\rho_f} + \frac{\varphi}{1 - \varphi}\right) - \frac{\varphi}{1 - \varphi}. \quad \text{(A11)}$$

Let

$$w = u\left(\frac{\rho_s}{\rho_l} + \frac{\varphi}{1 - \varphi}\right). \quad \text{(A12)}$$

The variation in m_{ex} with time is then given by

$$\frac{dm_{ex}}{dt} = we^{-ut}. \quad \text{(A13)}$$

The activity of the melt in the residuum is estimated using the equations (8), (9) and (10) given by Zou & Zindler (2000), which were first derived by McKenzie (1985). These equations estimate the activity of (^{238}U), (^{230}Th), and (^{226}Ra) in the residual melt. They are rather complicated, and the derivation is greatly simplified by approximating these activities by an exponential function, the approximations having regression coefficients better than 0·99. Hence, the initial activities R_i of the melts before ascent are here given by

$$(^{230}\text{Th}) = ae^{-\alpha t} \quad \text{(A14)}$$

$$(^{226}\text{Ra}) = be^{-\beta t}. \quad \text{(A15)}$$

There are two different periods of time involved: the period of time for partial melting of the mantle, and that for the ascent of the melt from the partially molten region. To perform the integration required, the time for the melt ascent should be expressed as a function of the time for partial melting. Let the maximum time for partial melting of a unit volume of the mantle be $\mathcal{T}_m$. The maximum period of time for ascent of the melt is $\mathcal{T}_a$. The mantle that has been molten for the time t delivers melt that ascends for a period of time s given by

$$s = \left(1 - \frac{t}{\mathcal{T}_m}\right)\mathcal{T}_a = \mathcal{T}_a - \frac{\mathcal{T}_a}{\mathcal{T}_m}t = p - qt. \quad \text{(A16)}$$

During the ascent of the melt the activities change. Using the decay equation for a daughter isotope given by Ivanowich [1982, equation (1.17)], the Ra activity in the accumulated extracted melt is estimated from

$$(^{226}\text{Ra}) = \frac{1}{W}\int\left(ae^{-\alpha t}we^{-ut}\frac{\lambda_{Ra}}{\lambda_{Ra} - \lambda_{Th}}[e^{-\lambda_{Th}(p-qt)} - e^{-\lambda_{Ra}(p-qt)}] + be^{-\beta t}we^{-ut}e^{-\lambda_{Ra}(p-qt)}\right)dt. \quad \text{(A17)}$$

For (^{230}Th) one obtains a similar equation:

$$(^{230}\text{Th}) = \frac{1}{W}\int(ae^{-\alpha t}we^{-ut}e^{-\lambda_{Th}(p-qt)})dt \quad \text{(A18)}$$

where W is the total amount of melt accumulated. Let

$$c_1 = \frac{aw\lambda_{Ra}}{\lambda_{Ra} - \lambda_{Th}} \quad \text{(A19)}$$

$$c_2 = bw$$

$$c_3 = aw.$$

The solutions for the activities are then given by

$$(^{226}\text{Ra}) = \frac{1}{W}\left(-\frac{c_1e^{-\lambda_{Th}p + (q\lambda_{Th} - \alpha - u)t}}{q\lambda_{Th} - \alpha - u} + \frac{c_1e^{-p\lambda_{Ra}}e^{(q\lambda_{Ra} - \alpha - u)t}}{q\lambda_{Ra} - \alpha - u} - \frac{c_2e^{-p\lambda_{Ra}}e^{(q\lambda_{Ra} - \beta - u)t}}{q\lambda_{Ra} - \beta - u}\right)\Bigg|_{t_c}^{t_c} \quad \text{(A20)}$$

$$(^{230}\text{Th}) = \frac{1}{W}\left(-\frac{c_3e^{-p\lambda_{Th}}e^{(q\lambda_{Th} - \alpha - u)t}}{q\lambda_{Th} - \alpha - u}\right)\Bigg|_{t_c}^{t_c}. \quad \text{(A21)}$$

The integration is performed between the times for the onset of melt extraction and the end of melt extraction, t_c and t_e, respectively. The activity ratio, R_a, of the accumulated melt is then given by

$$R_a = \frac{(^{226}\mathrm{Ra})}{(^{230}\mathrm{Th})}. \tag{A22}$$

As an example, for 20% partial melting by volume, a melting period of 400 kyr, a maximum period of time of 500 a for ascent of the melt and $\varphi = 0{\cdot}2\%$ give

$$\begin{aligned} a &= 0{\cdot}3367 & p &= 500 \\ \alpha &= 4{\cdot}5424 \times 10^{-5} & q &= 0{\cdot}00125 \\ b &= 0{\cdot}8131 & t_c &= 3263\mathrm{a} \\ \beta &= 4{\cdot}7028 \times 10^{-5} & u &= 5{\cdot}5786 \times 10^{-7}. \end{aligned} \tag{A23}$$

The initial $(^{226}\mathrm{Ra}/^{230}\mathrm{Th})$ of the melt at z_0 is given by $b/a = 2{\cdot}41$. The value of u is estimated for 20% melting by volume and $t = 400$ kyr. With the weight fraction, $3{\cdot}04 \times 10^{-8}\,\mathrm{cm}^{-1}$ estimated above, then 20% melting occurs within 65·8 km. The ascent rate of the mantle then becomes 16·5 cm/a. The maximum ascent distance within the partially molten mantle is 65·8 km, equivalent to an average melt ascent rate of 132 m/a.